Experimental and Theoretical Studies of the $C_6H_5 + C_6H_6$ Reaction

J. Park, S. Burova, A. S. Rodgers,† and M. C. Lin*

Department of Chemistry, Emory University, Atlanta, Georgia 30322

Received: June 21, 1999; In Final Form: September 7, 1999

The absolute rate constants for the $C_6H_5 + C_6H_6$ and C_6D_6 reactions have been measured by cavity ringdown spectrometry at temperatures between 298 and 495 K at a constant 40 Torr Ar pressure. The new results, which reveal no detectable kinetic isotope effect, can be represented by the Arrhenius equation, $k_1 = 10^{(11.91\pm0.13)} \exp[-(2102 \pm 106)/T]$ cm^3/(mol s). Our low-temperature data for the addition/stabilization process, $C_6H_5 + C_6H_6 \rightarrow C_{12}H_{11}$, can be correlated with those obtained in a low-pressure, high-temperature Knudsen cell study for the addition/displacement reaction, $C_6H_5 + C_6H_6 \rightarrow C_{12}H_{10} + H$, by the RRKM theory using the molecular and transition-state parameters computed at the B3LYP/6-311G(d,p) level of theory. Combination of these two sets of data gives $k_1 = 10^{(11.98\pm0.03)} \exp[-(2168 \pm 34)/T]$ cm^3/(mol s) covering the temperature range 298−1330 K. The RRKM theory also correlates satisfactorily the forward reaction data with the high-temperature shock-tube result for the reverse H-for-C_6H_5 substitution process with 2.7 and 4.7 kcal/mol barriers for the entrance ($C_6H_5 + C_6H_6$) and reverse ($H + C_{12}H_{10}$) reactions, respectively. For modeling applications, we have calculated the forward reaction rate constants for the formation of the two competing products, $H + C_{12}H_{10}$ and $C_{12}H_{11}$, at several pressures covering 300 K < T < 2500 K.

I. Introduction

The reaction of phenyl radical with benzene is of great importance to incipient soot formation chemistry and to the combustion of lead-free gasoline in which small aromatic hydrocarbons are key ingredients providing high-octane values. The kinetics of this reaction was first studied by Stein and coworkers[1,2] using a low-pressure Knudsen cell−mass spectrometric technique in the temperature range 1000−1330 K by monitoring the formation of biphenyl,

$$C_6H_5 + C_6H_6 \rightarrow C_{12}H_{10} + H \qquad (1)$$

They reported the expression, $k_1 = 3 \times 10^{12} \exp(-4300/T)$ cm^3/(mol s), assuming the rate constant for the recombination reaction of phenyl radicals,

$$C_6H_5 + C_6H_5 \rightarrow C_{12}H_{10} \qquad (2)$$

to be $k_2 = 3 \times 10^{12}$ cm^3/(mol s). Combination of their high-temperature, low-pressure data with that determined at room temperature in solution by Scaiano and Stewart[3] gave rise to the approximate expression, $k_1 = 4 \times 10^{11} \exp(-2000/T)$ cm^3/(mol s). A comparison of this and other data estimated earlier by kinetic modeling will be made later.

Recently, Manion and Tsang[4] measured the rate constant for the reverse process,

$$H + C_{12}H_{10} \rightarrow C_6H_5 + C_6H_6 \qquad (-1)$$

in a single-pulsed shock tube using $H + 1,3,5\text{-}(CH_3)_3C_6H_3$ as a reference reaction with hexamethyl ethane as the H atom source in the temperature range 1018−1135 K at pressures near 2 atm. This high-pressure, high-temperature result, with $k_{-1} = 4.1 \times 10^{13} \exp(-4418/T)$ cm^3/(mol s), is reported to be consistent with Fahr and Stein's low-pressure Knudsen cell data mentioned above.

The $C_6H_5 + C_6H_6$ reaction is believed to take place by an addition/elimination mechanism via the $C_{12}H_{11}$ (phenyl cyclohexadienyl radical) intermediate for both forward and reverse processes.[1−5] In view of the expected strong P,T effects on the stabilization vs decomposition of the excited intermediate under combustion conditions, because of the low stability of the cyclohexadienyl adduct,[6] we have carried out a theoretical study of the reaction using the combination of a hybrid density functional theory and the statistical Rice−Ramsperger−Kassel−Marcus (RRKM) theory calculations to correlate our low-temperature kinetic result, measured by the sensitive cavity ringdown technique,[7−11] with the aforementioned high-temperature data. The results of our experimental and theoretical studies covering a wide range of P,T conditions are presented in this article for combustion modeling applications.

II. Experimental Method

The cavity ringdown kinetic spectrometry (CRDS) technique has been described in detail elsewhere.[7−11] For C_6H_5 radical reactions, we have previously presented our reactor configuration, flow conditions, and radical detectivity in ref 9.

All experiments were performed under slow-flow conditions using Ar as the carrier gas to provide a total pressure of 40 Torr. The flow reactor consists of a heatable Pyrex glass tube attached with two pairs of laser windows opposite to each other, permitting the two-split photolysis laser beams to cross at the center of the reactor at a 30° angle. The reactor was vacuum-sealed at the ends with a pair of highly reflective mirrors (R = 0.9999 at 500 nm, radius curvature 6 m), which form a high quality optical cavity, approximately 0.5 m in length. The quality of the cavity is such that a pulse of probing dye laser operating at 500 nm with fwhm ≃10 ns can be lengthened to about 20 μs, providing an effective optical path of 6×10^3 m.

† Deceased.

* Corresponding author. E-mail address: chemmcl@emory.edu.

10.1021/jp9920592 CCC: $18.00
Published on Web 10/14/1999

Two pulsed lasers were employed, one for the generation of the C_6H_5 radical and the other for its detection. For radical generation, we employed a Lambda Physik LPX 100 excimer laser at 248 nm with C_6H_5NO as the precursor. For the probing of the C_6H_5 radical at 504.8 nm a Lambda Physik excimer laser pumped tunable dye laser was used. The photoelectric signal from the PMT was amplified with a fast preamplifier (SR445) and acquired and averaged with a multichannel digital oscilloscope (LeCroy 9310 M). The averaged signal was stored in a computer for future data analysis. A pulse-delay generator (SR DG 535) interfaced with the computer was employed to control the firing of the two lasers as well as the triggering of the data acquisition system.

The CRDS method measures the decay times of the injected probing photons in the absence (t_c^o) and the presence (t_c) of absorbing species. These photon decay times can be related to the concentration of the species at time t' after its generation by the equation[6−11]

$$1/t_c = 1/t_c^o + B[A]_o e^{-k't'} \quad \text{(Ia)}$$

or

$$\ln(1/t_c - 1/t_c^o) = C - k't' \quad \text{(Ib)}$$

where $[A]_o$ is the initial concentration of the radical species of interest, C_6H_5, B is a constant which contains experimental parameters such as the cavity length (50 cm), the refractive index of the absorbing medium, etc., and $C = \ln(B[A]_0)$. Equation Ia or Ib is valid provided that the decay time of the species of interest is much longer than that of photons within the cavity. This condition can be readily met because the chemical decay time, typically in the range of several tens of milliseconds, can be controlled by the concentration of the molecular reagent.

The slopes of the $\ln(1/t_c - 1/t_c^o)$ vs t' plots for the reaction of C_6H_5 with C_6H_6 yield the pseudo-first-order rate coefficients, k', for the decay of C_6H_5 in the presence of known, excess C_6H_6 concentrations as specified. A standard plot of k' vs reagent concentration gives the averaged second-order rate constant k'' from its slope according to the relationship

$$k' = k^o + k_x''[X] \quad \text{(II)}$$

where k^o is the radical decay constant in the absence of the molecular reactant X due to the loss of the radical by diffusion away from the probing beam and recombination reactions (e.g., $C_6H_5 + NO$ and $C_6H_5 + C_6H_5$).

C_6H_5NO and C_6H_6 were obtained from Aldrich. C_6H_5NO was recrystallized using ethanol as solvent and vacuum-dried before use, and C_6H_6 was purified by standard trap-to-trap distillation. Ar carrier gas (Specialty Gases, 99.995%) was used without further purification.

III. Theoretical Calculations

As the abstraction reaction does not transform the reactants in the present case, the only mechanism, which leads to the formation of biphenyl, takes place by the following addition−elimination process:

$$C_6H_5 + C_6H_6 \leftrightarrow C_{12}H_{11} \leftrightarrow C_{12}H_{10} + H \quad (1,-1)$$

To confirm the mechanism, we have employed a hybrid density functional theory, B3LYP, to calculate the relative energy of the adduct, as well as those of the two transition states, TS1 and TS2, associated with the initial addition and the elimination of the H atom, respectively. The B3LYP method utilizes Becke's three-parameter nonlocal exchange functional[12] with the nonlocal correlation function of Lee, Yang, and Parr.[13] The B3LYP method is known to be reliable for prediction of molecular structures and their vibrational frequencies (which require no scaling to match experimental values).[14]

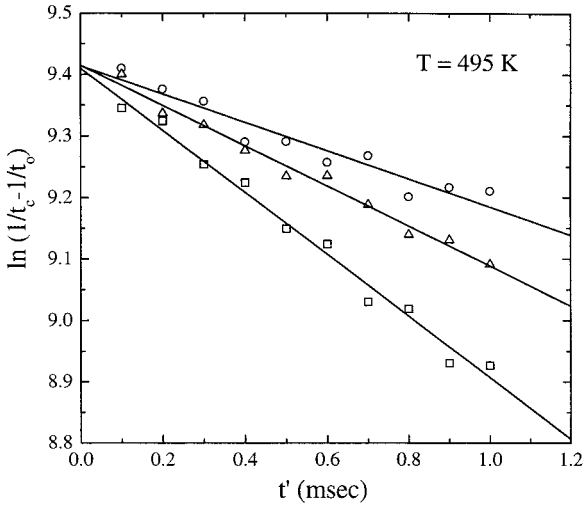

Figure 1. Typical pseudo-first-order decay plots of C_6H_5 measured under various conditions at 495 K: (○) $[C_6H_6] = 0$; (△) $[C_6H_6] = 0.24$ Torr; (□) $[C_6H_6] = 0.63$ Torr.

Because of the large molecular size involved in the present system, we used the moderate Gaussian basis set, 6-31G(d,p),[15] for initial geometry optimization and transition-state search. The calculation was repeated with a larger 6-311G(d,p)[15] basis set. The result of these calculations will be discussed in the following section.

The observed kinetic data, including those obtained in earlier studies as reviewed in the Introduction, will be interpreted and correlated with the standard RRKM theory involving a single long-lived intermediate[16−18] based on the result of the quantum chemical calculation mentioned above.

IV. Results and Discussion

Experimental Results. A typical set of pseudo-first-order plots, $\ln(1/t_c - 1/t_c^o)$ vs time, for the C_6H_5 reaction with C_6H_6 is presented in Figure 1. The slopes of these plots give the apparent first-order decay constants (k') for the specific concentrations of the molecular reactant present in the system. Figure 2 illustrates the dependence of k' on C_6H_6 concentration as depicted by eq II. From the slope of the second-order plot for each temperature, we obtain the total bimolecular rate constant for the reaction, $C_6H_5 + C_6H_6 \rightarrow$ products, $k_1 = 10^{(11.91\pm0.13)} \exp[-(2102 \pm 106)/T]$ cm^3/(mol s).

Table 1 summarizes the bimolecular rate constants obtained by CRDS, and the result revealed no detectable kinetic isotope effect on the measured rate constants. These results are graphically presented in Figure 3 together with Fahr and Stein's low-pressure data.[1,2] These data were re-evaluated by using our reported C_6H_5 recombination rate constant $k_2 = 1.39 \times 10^{13} \exp(-55/T)$ cm^3/(mol s).[19] A weighted least-squares analysis[20] including these two sets of data gave rise to

$$k_1 = 10^{(11.98\pm0.03)} \exp[-(2168 \pm 34)/T] \text{ cm}^3/(\text{mol s}) \quad \text{(IV)}$$

The validity of this analysis is discussed below. Also included in Figure 3 is the room-temperature result of Scaiano and

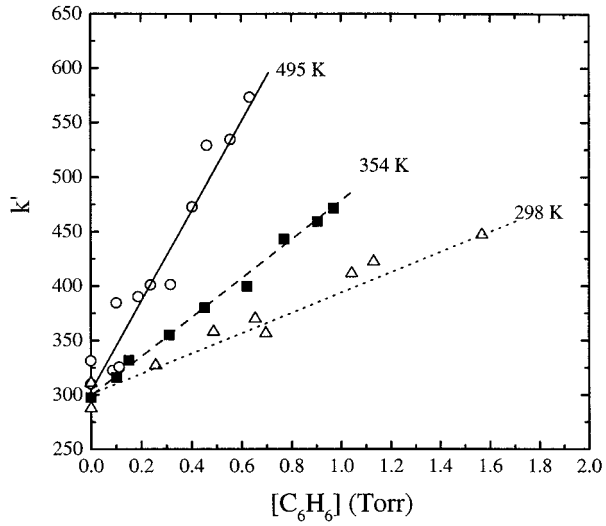

Figure 2. k' vs $[C_6H_6]$ for the $C_6H_5 + C_6H_6$ reaction measured at the specified temperatures.

TABLE 1: Measured Bimolecular Rate Constants of C_6H_5 Reactions with C_6H_6 and C_6D_6[a]

reactant	T (K)	[RH] (10^{-8} mol/cm^3)	k_1 (cm^3 mol^{-1} s^{-1})[b]
C_6H_6	298	0−9.88	$(5.70 \pm 3.79) \times 10^8$
C_6H_6	320	0−6.52	$(1.27 \pm 0.48) \times 10^9$
C_6D_6	333	0−4.42	$(1.54 \pm 0.85) \times 10^9$
C_6H_6	354	0−4.10	$(2.43 \pm 0.67) \times 10^9$
C_6H_6	375	0−3.44	$(2.86 \pm 1.10) \times 10^9$
C_6H_6	411	0−3.56	$(5.06 \pm 1.60) \times 10^9$
C_6D_6	426	0−3.16	$(6.12 \pm 1.62) \times 10^9$
C_6H_6	495	0−2.05	$(1.03 \pm 0.31) \times 10^{10}$

[a] All experiments were carried out with a total pressure of 40 Torr using Ar as the carrier gas. [b] The uncertainties represent 1σ, evaluated by weighted least-squares analysis, convoluting the errors from the determination of k' and k''.

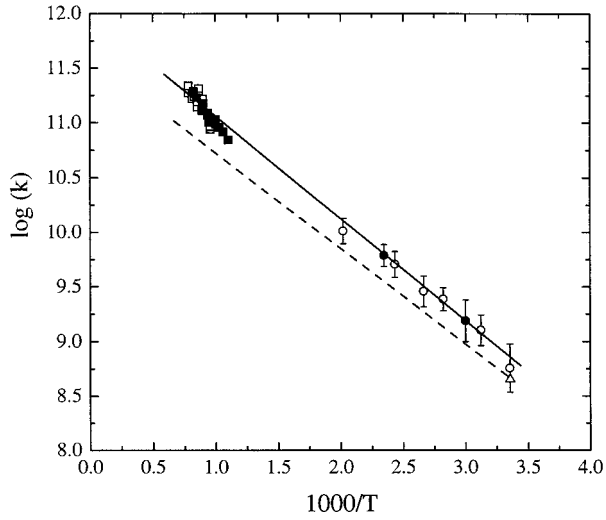

Figure 3. Arrhenius plot for $C_6H_5 + C_6H_6$ (○) and C_6D_6 (●): (□) and (■), ref 1 and ref 2 (both data were rescaled using our phenyl radical recombination data (ref 19); (△), ref 3. Solid line, least-squares fitting in combination with those rescaled data of ref 1; dashed line, ref 1 ($k_1 = 4 \times 10^{11} \exp(-2000/T)$ cm^3 mol^{-1} s^{-1}).

Stewart,[3] $(4.5 \pm 0.3) \times 10^8$ cm^3/(mol s), which agrees with our value within the cited experimental errors (see Table 1).

RRKM Calculations. We have performed RRKM calculations for the formation and decomposition of the excited phenyl cyclohexadienyl adduct, $C_{12}H_{11}^{\#}$, to correlate the forward and reverse rate constants measured under varying T,P conditions according to the following scheme:

$$C_6H_5 + C_6H_6 \underset{-a}{\overset{a}{\rightleftharpoons}} C_{12}H_{11}^{\#} \underset{-b}{\overset{b}{\rightleftharpoons}} C_{12}H_{10} + H \quad (1,-1)$$

$$\overset{c}{\rightarrow} C_{12}H_{11} (+ M)$$

where "#" represents internal excitation and M denotes a third body (i.e., a molecular quencher). Figure 4 presents the geometries of all molecular species, the radical adduct, and the transition states involved in the reaction calculated at the B3LYP/6-311G(d,p) level of theory. The potential energy curve of the system predicted at the B3LYP/6-311G(d,p) level of theory is shown by the dashed curve in Figure 5. The molecular parameters for the reactants, the adduct, and the bipheny product are summarized in Table 2; these parameters will be used in the RRKM calculations discussed below.

TABLE 2: Molecular and Transition-State Parameters of the Reactants, Products, and Transition States of the $C_6H_5 + C_6H_6 = C_{12}H_{10} + H$ Reaction, Calculated at the B3LYP/6-311G(d,p) Level

species	I_i (10^{-40} g cm^2)	ν_j (cm^{-1})
C_6H_5	134.3 150.3 284.6	400, 426, 602, 620, 673, 721, 812, 892, 964, 989, 993, 1017, 1050, 1073, 1175, 1176, 1302, 1324, 1463, 1471, 1576, 1630, 3156, 3162, 3174, 3177, 3188
C_6H_6	148.0 148.0 296.1	412, 412, 623, 623, 687, 723, 861, 861, 980, 980, 1014, 1015, 1024, 1061, 1061, 1175, 1198, 1198, 1336, 1382, 1513, 1513, 1638, 1638, 3156, 3166, 3166, 3181, 3181, 3192
$C_{12}H_{10}$	294.6 1549.1 1772.5	66, 95, 127, 269, 313, 369, 414, 420, 504, 559, 627, 629, 641, 714, 717, 756, 757, 798, 857, 858, 924, 942, 981, 983, 1002, 1002, 1012, 1018, 1026, 1054, 1067, 1102, 1107, 1182, 1183, 1203, 1210, 1298, 1303, 1327, 1355, 1359, 1462, 1490, 1516, 1538, 1610, 1626, 1644, 1646, 3159, 3160, 3165, 3168, 3175, 3179, 3181, 3184, 3190, 3191
$C_{12}H_{11}$	344.8 1516.9 1551.4	26(a), 63, 107, 232, 275, 305, 405, 415, 498, 541, 588, 593, 625, 636, 692, 715, 744, 779, 781, 850, 857, 901, 927, 967, 974, 979, 990, 997, 1001, 1018, 1024, 1051, 1101, 1115, 1174, 1181, 1191, 1202, 1204, 1230, 1289, 1339, 1347, 1360, 1398, 1450, 1483, 1524, 1539, 1598, 1626, 1642, 2898, 3152, 3153, 3154, 3161, 3170, 3173, 3174, 3178, 3188, 3194
TS1	388.0 1571.9 1660.6	329i, 13(a), 63, 64, 144, 155, 366, 398, 412, 443, 567, 613, 616, 616, 682, 692, 721, 728, 834, 839, 866, 898, 900, 965, 976, 986, 989, 994, 1007, 1019, 1033, 1044, 1051, 1059, 1080, 1171, 1176, 1178, 1183, 1195, 1319, 1324, 1325, 1375, 1464, 1477, 1491, 1501, 1583, 1585, 1606, 1627, 3141, 3153, 3157, 3161, 3165, 3165, 3169, 3181, 3183, 3184, 3192
TS2	305.7 1557.4 1765.8	947i, 61, 98, 123, 255, 306, 364, 400, 417, 458, 512, 552, 569, 625, 635, 639, 697, 714, 743, 769, 799, 843, 854, 920, 936, 979, 981, 998, 1001, 1002, 1017, 1024, 1046, 1062, 1100, 1108, 1179, 1182, 1201, 1207, 1284, 1288, 1323, 1353, 1355, 1459, 1487, 1503, 1530, 1586, 1621, 1625, 1644, 3160, 3162, 3166, 3169, 3176, 3181, 3183, 3187, 3191, 3193

[a] These modes are treated as free internal rotors with the reduced moment of inertia, 25.16 for $C_{12}H_{11}$ and 27.46 for TS1 in units of 10^{-40} g cm^2.

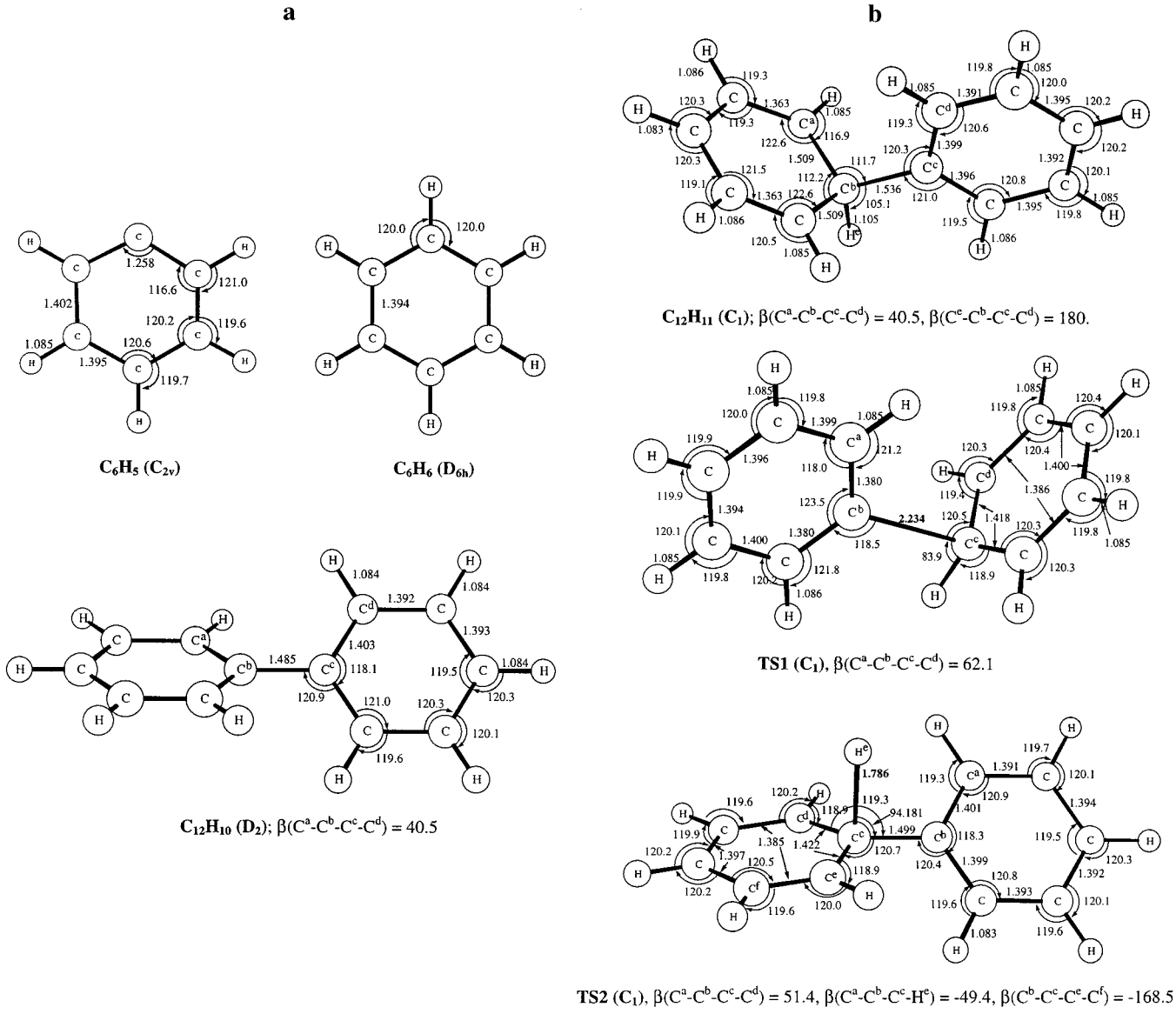

Figure 4. Molecular and transition state geometries, optimized at the B3LYP/6-311G(d,p) level of theory. Bond lengths are in angstroms and angles in degrees. All C−H bond lengths are 1.084 Å unless otherwise noted.

In view of the fact that the hybrid density functional theory predicts reaction energies with only semiquantitative reliability,[14] particularly for the large systems such as the present one, we have carried out isodesmic calculations for biphenyl and the $C_{12}H_{11}$ adduct using the following two reactions:

$$C_6H_5C_2H_3 + C_6H_6 = C_{12}H_{10} + C_2H_4 \quad (2)$$

$$C_{12}H_{10} + C_6H_7 = C_{12}H_{11} + C_6H_6 \quad (3)$$

Reaction 2 is employed to test the reliability of the scheme, while reaction 3 is utilized to evaluate the heat of formation of the adduct using that of C_6H_7 (cyclohexadienyl radical) predicted by the G2M method.[6] The heats of formation of molecular species used in the two isodesmic reactions are known;[21] their values, corrected to 0 K using the molecular parameters given in Table 2, are listed in the footnote of Table 3.

The predicted heats of formation of biphenyl and the radical adduct presented in Table 3 were based on the energies computed at the B3LYP/6-31G(d,p) and B3LYP/6-311G(d,p) levels. For biphenyl, the isodesmic calculations with the two different basis sets give 46.0 and 50.2 kcal/mol, respectively. The latter obtained with the larger basis set agrees exactly with the experimental value[21] extrapolated to 0 K. With the same bigger basis set, the isodesmic calculation using reaction 3 predicts the relative energy of the adduct to the $C_6H_5 + C_6H_6$ reactants, −22.6 kcal/mol, which is more stable than those predicted by B3LYP/6-31G(d,p) and 6-311G(d,p), −19.3 and −17. 3 kcal/mol, respectively, as given in Table 3. For RRKM calculations, the isodesmic results for $C_{12}H_{11}$ (−22.6 kcal/mol) and for the overall exothermicity of reaction 1 (−6.5 kcal/mol) were used.

The RRKM calculations were carried out with our existing computer programs formerly employed for interpretation of the $CH_3 + O_2$,[16] $CH + N_2$,[17] and $H + N_2O$[18] reactions. For the former two reactions, coupled reaction channels were solved by the standard steady-state treatment, whereas for the latter process, the master equation coupling the entrance and exit channels with tunneling corrections was solved by a matrix method.[18] Both programs were employed to test the effect of quantum mechanical tunneling on the production of $C_{12}H_{10} + H$. The effect was found to be negligible because of the relatively low exit barrier comparing with the entrance one (vide infra).

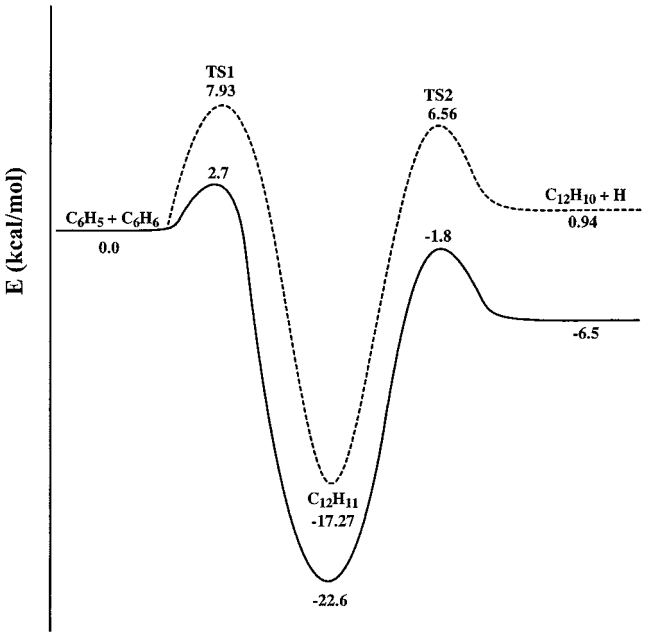

Figure 5. Calculated and fitted potential energy profiles based on the calculation at the B3LYP/6-311G(d,p) level for the $C_6H_5 + C_6H_6 \rightarrow C_{12}H_{11} \rightarrow C_{12}H_{10} + H$ reaction.

TABLE 3: Thermochemistry of the $C_6H_5 + C_6H_6 = C_{12}H_{10} + H$ Reaction[a]

	ΔH_r^o	ΔH_f° ($C_{12}H_{10}$)	ΔH_f° ($C_{12}H_{11}$)[b]
experiment	−6.49	50.18	
B3LYP/6-31G(d,p)	−0.70		−19.32
B3LYP/6-311G(d,p)	0.94		−17.27
isodesmic (I) 6-31G(d,p)		45.96	
(II) 6-311G(d,p)		50.22	−22.59

[a] All energies are given in kcal/mol. The 0 K heats of formation used in the isodesmic calculations are: C_2H_4, 14.6; C_6H_6, 24.0; $C_6H_5C_2H_3$, 39.2; C_6H_7, 55.4. The source references are cited in the text. [b] Relative to the $C_6H_5 + C_6H_6$ reactants.

On account of the lack of reliability in the predicted reaction energies at the present level of theory, the energy barriers for the forward addition ($C_6H_5 + C_6H_6$), E_a°, and the reverse addition ($H + C_{12}H_{10}$), E_{-b}°, were adjusted to fit the experimental values of k_1 and k_{-1}. For the evaluation of E_a°, our low-temperature (298−498 K), high-pressure k_1 data provide a direct determination of the barrier, because the rate constants are effectively in the *P*-independent region. As illustrated in Figure 6a, our 40 Torr experimental data agree exactly with the high-*P* curve at temperature below 500 K. Under our conditions, reaction 1 produces exclusively the thermalized adduct by collisional deactivation. The value of the entrance barrier, which fits most satisfactorily the C_6H_5 decay rate constants measured by CRDS, is $E_a^\circ = 2.7$ kcal/mol. The dominance of the addition−stabilization mechanism under our experimental conditions explains the absence of kinetic isotope effect in the C_6D_6 reaction.

On the other hand, under the high-temperature (1000−1330 K) and low-pressure (1−10 mTorr) conditions employed by Fahr and Stein in their Knudsen cell study,[1,2] the reaction takes place exclusively by H-displacement via (1b); its rate constant is not only affected by E_a° but also by E_{-b}° which influences the rates of both the forward H atom elimination (1b) and the competitive redissociation (−1a). Similarly, for the overall reverse process, $H + C_{12}H_{10} \rightarrow C_6H_5 + C_6H_6$ (−1), the rate constant reported by Manion and Tsang[4] was found to be pressure dependent and influenced strongly by both E_{-b}° and E_a° on account of the large

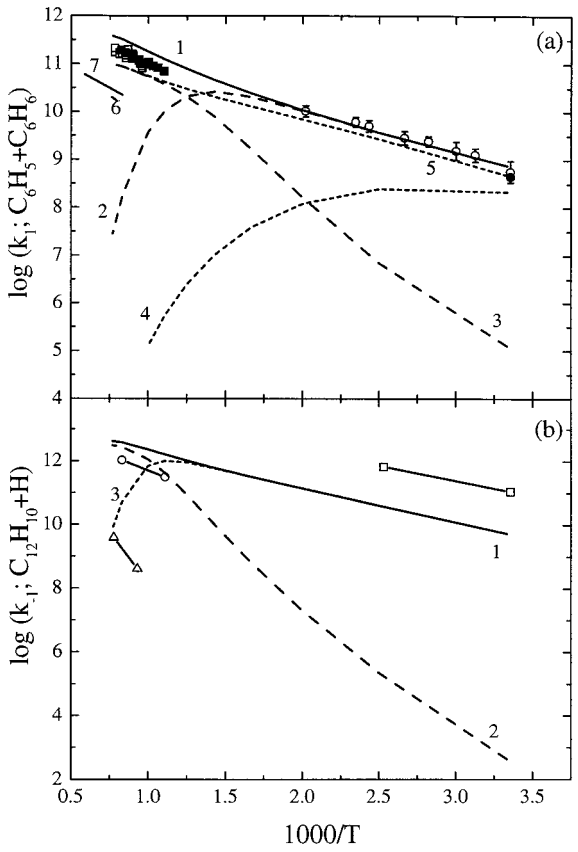

Figure 6. Comparison of the experimental and theoretically predicted results for $C_6H_5 + C_6H_6 \leftrightarrow C_{12}H_{10} + H$ in the forward and reverse directions. (a) 1, k_{tot} (inf); 2, $k_{C_{12}H_{11}}$ (40 Torr); 3, $k_{C_{12}H_{10}+H}$ (40 Torr); 4, $k_{C_{12}H_{11}}$ (10 mTorr); 5, $k_{C_{12}H_{10}+H}$ (10 mTorr); 6, ref 22; 7, ref 23. All data points are given in Figure 3. (b) 1, k_{tot}; 2, $k_{C_6H_5+C_6H_6}$ (2 atm); 3, $k_{C_{12}H_{11}}$ (2 atm); (○) ref 4; (□) ref 24; (△) ref 25.

endothermicity for the reaction (−6.5 kcal/mol). By fitting both Fahr and Stein's data for biphenyl formation from $C_6H_5 + C_6H_6$ and Manion and Tsang's results for benzene production from $H + C_{12}H_{10}$, we obtained $E_{-b}^\circ = 4.7$ kcal/mol. The calculated rate constants using the modified PES shown in Figure 5 by the solid curve are presented in Figure 6a for the forward process and Figure 6b for the reverse process, for comparison with experimental data determined under different conditions. In these figures, we also include other data obtained indirectly by either kinetic modeling or thermochemical estimation for the sake of completeness.

As shown in Figure 6, the high-temperature experimental data determined directly for the forward[1,2] and reverse[4] reactions can be reasonably correlated with our low-temperature results by the RRKM theory, using the molecular parameters (i.e., moments of inertia and vibrational frequencies) and the energy of the adduct afforded by quantum calculations. For the reverse $H + C_{12}H_{10}$ reaction, the overall barrier for the production of C_6H_6, is 6.5 + 2.7 = 9.2 kcal/mol; it is close to Manion and Tsang's apparent activation energy, 8.8 kcal/mol, measured near 1000 K at about 2 atm pressure.[4] Under their experimental conditions, the stabilization of the excited $C_{12}H_{11}$ adduct and the production of benzene are competitive. Accordingly, the radical adduct may participate in other reactions, such as the scavenging of H atoms by the process $H + C_{12}H_{11} \rightarrow H_2 + C_{12}H_{10}$.

The forward and reverse addition barriers, $E_a^\circ = 2.7$ and $E_{-b}^\circ = 4.7$ kcal/mol, appear to be reasonable. For the C_6H_5 addition process, we have measured by CRDS the activation energies

TABLE 4: Effects of Temperature and Pressure on the Rate Constant[a] for the $C_6H_5 + C_6H_6$ Reaction[a]

T (K)	k_{1b} 10 mTorr	k_{1c} 10 mTorr	k_{1b} 40 Torr	k_{1c} 40 Torr	k_{1b} 1 atm	k_{1c} 1 atm	k_{1b} 2 atm	k_{1c} 2 atm	k_{1b} 10 atm	k_{1c} 10 atm
300	4.79×10^{8}	2.14×10^{8}	1.27×10^{5}	7.59×10^{8}	6.69×10^{3}	7.59×10^{8}	3.35×10^{3}	7.59×10^{8}	6.69×10^{2}	7.59×10^{8}
500	6.93×10^{9}	1.20×10^{8}	1.60×10^{8}	1.05×10^{10}	9.76×10^{6}	1.08×10^{10}	4.90×10^{6}	1.08×10^{10}	9.82×10^{5}	1.08×10^{10}
700	2.04×10^{10}	1.01×10^{7}	7.83×10^{9}	2.60×10^{10}	1.30×10^{9}	4.24×10^{10}	7.29×10^{8}	4.40×10^{10}	1.66×10^{8}	4.55×10^{10}
1000	5.51×10^{10}	1.23×10^{5}	5.37×10^{10}	3.70×10^{9}	4.34×10^{10}	3.36×10^{10}	3.81×10^{10}	5.00×10^{10}	2.26×10^{10}	1.00×10^{11}
1500	8.43×10^{10}	1.27×10^{1}	8.43×10^{10}	5.09×10^{5}	8.43×10^{10}	9.70×10^{6}	8.43×10^{10}	1.93×10^{7}	8.43×10^{10}	9.64×10^{7}
2000	8.01×10^{9}	1.37×10^{-4}	8.01×10^{9}	5.46×10^{0}	8.01×10^{9}	1.04×10^{2}	8.01×10^{9}	2.07×10^{2}	8.01×10^{9}	1.04×10^{3}
2500	1.62×10^{8}	6.20×10^{-10}	1.62×10^{8}	2.49×10^{-5}	1.62×10^{8}	4.73×10^{-4}	1.62×10^{8}	9.46×10^{-4}	1.62×10^{8}	4.73×10^{-3}

[a] In units of cm^3/(mol s). k_{1b} and k_{1c} represent the formation of $C_{12}H_{10} + H$ and $C_{12}H_{11}$, respectively.

for the reactions with C_2H_2[26] and C_2H_4[27], 3.1 and 4.5 kcal/mol, respectively. They are comparable with the 4.0 kcal/mol value for the C_6H_6 reaction. For the $H + C_{12}H_{10}$ addition process, the value of $E_{-b}°$ is about half that of $H + C_6H_6$,[6] 8.9 kcal/mol. This large difference in the addition barriers may be attributed in part to the large activation energy needed to overcome the resonance stabilization in C_6H_6 and in part to the retention of some resonance energy in $C_{12}H_{11}$ across the two π-systems (i.e., the two C_6 rings).

For practical kinetic modeling, we have calculated the rate constants for the two branching reactions, (1b) and (1c), at different pressures covering the temperature range 300−2500 K. They are summarized in Table 4. The equilibrium constant for the overall process, $C_6H_5 + C_6H_6 = C_{12}H_{10} + H$, $K_1 = 1.45 \times 10^{-13}\ T^{3.23} \exp(3998/T)$, may be used to convert these rate constants for the reverse displacement reaction.

V. Conclusion

The kinetics of the $C_6H_5 + C_6H_6$ and C_6D_6 reactions has been investigated by cavity ringdown spectrometry at temperatures between 298 and 495 K at 40 Torr Ar pressure, with no detectable kinetic isotope effect on the measured rate constants. The results of RRKM calculations using the molecular and transition-state parameters computed at the B3LYP/6-311G(d,p) level of theory indicate that under our experimental conditions the measured bimolecular rate constants correspond exclusively to the formation of the phenyl cyclohexadienyl radical, fully consistent with the absence of kinetic isotope effect. These data can be quantitatively correlated with the rescaled data of Fahr and Stein[1,2] obtained by a low-pressure, high-temperature Knudsen cell study which determines exclusively the rate constant for the formation of biphenyl. A least-squares analysis of the two sets of kinetic data covering 298−1330 K gives $k_1 = 10^{(11.98\pm0.03)} \exp[-(2168 \pm 34)/T]$ cm^3/(mol s). These data and those of Manion and Tsang[4] measured for the reverse H-for-C_6H_5 substitution reaction using a single-pulse shock tube can be reasonably correlated by the RRKM theory with 2.7 and 4.7 kcal/mol for the entrance ($C_6H_5 + C_6H_6$) and reverse ($H + C_{12}H_{10}$) reaction barriers, respectively. For modeling applications, we have calculated the rate constants for the formation of the two competing product channels, $H + C_{12}H_{10}$ and $C_{12}H_{11}$, for several pressures covering 300 K < T < 2500 K.

Acknowledgment. The authors are grateful for the support of this work from the Basic Energy Sciences, Department of Energy, under Contract DE-FG02-97-ER14784. We are also thankful to Dr. W. H. Kirchhoff for providing us NERSC CPU time for the quantum chemical calculations.

References and Notes

(1) Fahr, A.; Stein, S. E. *22nd Symposium (International) on Combustion*; The Combustion Institute: Pittsburgh, PA, 1989; p 1023.
(2) Fahr, A.; Mallard, W. G.; Stein, S. E. *21st Symposium (International) on Combustion*; The Combustion Institute: Pittsburgh, PA, 1988; p 825.
(3) Scaiano, J. C.; Stewart, L. C. *J. Am. Chem. Soc.* **1983**, *105*, 3609.
(4) Manion, J. A.; Tsang, W. Proceedings of Chemical and Physical Processes in Combustion; 1996 Fall Technical Meeting, p 527.
(5) Louw, R.; Lucas, H. J. *Recl. Trav. Chim.* **1973**, *92*, 55.
(6) Mebel, A. M.; Lin, M. C.; Yu, T.; Morokuma, K. *J. Phys. Chem. A* **1997**, *101*, 3189.
(7) Yu, T.; Lin, M. C. *J. Am. Chem. Soc.* **1993**, *115*, 4371.
(8) Lin, M. C.; Yu, T. *Int. J. Chem. Kinet.* **1993**, *25*, 875.
(9) Yu, T.; Lin, M. C. *J. Phys. Chem.* **1994**, *98*, 2105.
(10) Park, J.; Chakraborty, D.; Lin, M. C. *J. Phys. Chem.* **1999**, *103*, 4003.
(11) Park, J.; Lin, M. C. *American Chemical Society Special Publication Series on Cavity Ringdown Spectroscopy*; American Chemical Society: Washington, DC, 1999; Chapter 13, p 196.
(12) (a) Becke, A. D. *J. Chem. Phys.* **1993**, *98*, 5648. (b) Becke, A. D. *J. Chem. Phys.* **1992**, *96*, 2155. (c) Becke, A. D. *J. Chem. Phys.* **1992**, *97*, 9173.
(13) Lee, C.; Yang, W.; Parr, R. G. *Phys. Rev. B* **1988**, *37*, 785.
(14) Mebel, A. M.; Morokuma, K, Lin, M. C. *J. Chem. Phys.* **1995**, *103*, 7414.
(15) Frisch, M. J.; Trucks, G. W.; Schlegel, H. B.; Gill, P. M. W.; Johnson, B. G.; Robb, M. A.; Cheeseman, J. R.; Keith, T.; Petersson, G. A.; Montgomery, J. A.; Raghavachari, K.; Al-Laham, M. A.; Zakrzewski, V. G.; Ortiz, J. V.; Foresman, J. B.; Cioslowski, J.; Stefanov, B. B.; Nanayakkara, A.; Challacombe, M.; Peng, C. Y.; Ayala, P. Y.; Chen, W.; Wong, M. W.; Andres, J. L.; Replogle, E. S.; Gomperts, R.; Martin, R. L.; Fox, D. J.; Binkley, J. S.; Defrees, D. J.; Baker, J.; Stewart, J. P.; Head-Gordon, M.; Gonzalez, C.; Pople, J. A. *Gaussian 94*, revision D.3; Gaussian, Inc.: Pittsburgh, PA, 1995.
(16) Hsu, D. S. Y.; Shaub, W. M.; Creamer, T.; Gutman, D.; Lin, M. C. *Ber. Bunsen-Ges. Phys. Chem.* **1983**, *87*, 909.
(17) Berman, M. R.; Lin, M. C. *J. Phys. Chem.* **1983**, *87*, 3933.
(18) Diau, E. M. G.; Lin M. C. *J. Phys. Chem.* **1995**, *99*, 6589.
(19) Park, J.; Lin, M. C. *J. Phys. Chem.* **1997**, *101*, 14.
(20) Cvetanovic, R. J.; Singleton, D. L.; Paraskevopoulos, G. *J. Phys. Chem.* **1979**, *83*, 50.
(21) Stull, D. R.; Westrum, E. F., Jr.; Sinke, G. C. *The Chemical Theromodynamics of Organic Compounds*; John Wiley & Sons: New York, 1969.
(22) Weissman, M.; Benson, S. W. *Int. J. Chem. Kinet.* **1984**, *16*, 307.
(23) Sauer, M. C., Jr.; Mani, I. *J. Phys. Chem.* **1970**, *74*, 59.
(24) Asaba, T.; Fujii, N. *Proc. Int. Symp. Shock Tubes Waves* **1971**, *8*, 1.
(25) Ritter, E. R.; Bozzelli, J. W.; Dean, A. M. *J. Phys. Chem.* **1990**, *94*, 2493.
(26) Yu, T.; Lin, M. C.; Melius, C. F. *Int. J. Chem. Kinet.* **1994**, *26*, 1095.
(27) Yu, Y.; Lin, M. C. *Combust. Flame* **1995**, *100*, 169.